Voltammetric Studies of the Catalytic Mechanism of the Respiratory Nitrate Reductase from *Escherichia coli*: How Nitrate Reduction and Inhibition Depend on the Oxidation State of the Active Site†

Sean J. Elliott,‡,§,|| Kevin R. Hoke,‡,§ Kerensa Heffron,§ Monica Palak,⊥ Richard A. Rothery,⊥ Joel H. Weiner,⊥ and Fraser A. Armstrong*,§

Inorganic Chemistry Laboratory, University of Oxford, South Parks Road, Oxford OX1 3QR, England, and Department of Biochemistry, 474 Medical Science Building, University of Alberta, Edmonton, Alberta T6G 2H7, Canada

Received October 17, 2003; Revised Manuscript Received November 14, 2003

ABSTRACT: The respiratory molybdoenzyme nitrate reductase (NarGHI) from *Escherichia coli* has been studied by protein film voltammetry, with the enzyme adsorbed on a rotating disk pyrolytic graphite edge (PGE) electrode. Catalytic voltammograms for nitrate reduction show a complex wave consisting of two components that vary with pH, nitrate concentration, and the presence of inhibitors. At micromolar levels of nitrate, the activity reaches a maximum value at approximately −25 mV and then decreases as the potential becomes more negative. As the nitrate concentration is raised, the activity at more negative potentials increases and eventually becomes the dominant feature at millimolar concentrations. This leads to the hypothesis that nitrate binds more tightly to Mo(V) than Mo(IV), so that low levels of nitrate are more effectively reduced at a higher potential despite the lower driving force. However, an alternative interpretation, that nitrate binding is affected by a change in the redox state of the pterin, cannot be ruled out. This proposal, *implicating a specific redox transition at the active site*, is supported by experiments carried out using the inhibitors azide and thiocyanate. Azide is the stronger inhibitor of the two, and each inhibitor shows two inhibition constants, one at high potential and one at low potential, both of which are fully competitive with nitrate; closer analysis reveals that the inhibitors act preferentially upon the catalytic activity at high potential. The unusual potential dependence therefore derives from the weaker binding of nitrate or the inhibitors to a more reduced state of the active site. The possible manifestation of these characteristics in vivo has interesting implications for the bioenergetics of *E. coli*.

Escherichia coli and many other facultative anaerobic bacteria possess the ability to utilize several simple oxides as terminal oxidants (*1*). Depending on their availability, nitrate, dimethyl sulfoxide (DMSO),[1] and trimethylammonium *N*-oxide (TMAO) can each serve as terminal electron acceptors in *E. coli*, in which their reduction, represented generically by eq 1, is catalyzed by the respective enzymes:

$$XO + 2e^- + 2H^+ \rightarrow X + H_2O \qquad (1)$$

nitrate reductase, DMSO reductase, and TMAO reductase. The catalytic, substrate-reducing subunits of these enzymes contain a Mo cofactor, in which a Mo atom is coordinated by two special dithiolene ligands, each of which is joined to a pterin group. The entire cofactor is referred to as molybdobis(molybdopterin−guanine dinucleotide), commonly abbreviated as Mo-bisMGD. These enzymes are also closely related to the well-characterized soluble DMSO reductase from *Rhodobacter* (*2*). The enzyme NarGHI is bound at the inner face of the cytoplasmic membrane where it couples the reduction of nitrate to nitrite with the oxidation of membrane-bound quinol and proton translocation by a redox loop mechanism (*3*−*5*). Respiratory nitrate reduction in *E. coli* is further complicated by the existence of two other nitrate reductases, NapAB and NarZYV. NapAB is a soluble periplasmic enzyme which accepts electrons from a membrane-bound *c*-type cytochrome (NapC) (*3*, *4*). NarZYV is a

† This work was funded by the Human Frontiers Science Program, EMBO, and BBSRC (43/10492). S.J.E. thanks EMBO for the award of a fellowship.

* To whom correspondence should be addressed.

‡ These authors contributed equally to this work.

§ University of Oxford.

|| Current address: Department of Chemistry, Boston University, 590 Commonwealth Ave., Boston, MA 02215.

⊥ University of Alberta.

[1] Abbreviations: A, electrode area; DMSO, dimethyl sulfoxide; *E*, electrode potential; EDTA, ethylenediaminetetraacetic acid; EPR, electron paramagnetic resonance; F, Faraday constant; FdnGHI, formate dehydrogenase; Γ, coverage of enzyme on the electrode (mol cm^{-2}); HEPES, *N*-(2-hydroxyethyl)piperazine-*N*′-2-ethanesulfonic acid; *i*, current; i_{lim}, limiting current at high driving force; k_{cat}, rate constant for catalytic turnover; K_M, Michaelis−Menten constant; K_d, dissociation constant of inhibitor; MES, 2-(*N*-morpholino)ethanesulfonic acid; MGD, molybdopterin−guanine dinucleotide; MOPS, 3-(*N*-morpholino)propanesulfonic acid; *n*, stoichiometric number of electrons transferred in an electrode process; NapAB, periplasmic nitrate reductase; NarGHI, cytoplasmic nitrate reductase; NarGH-His$_6$, His-tagged construct of NarGH; PGE, pyrolytic graphite edge; *R*, gas constant; SDS−PAGE, sodium dodecyl sulfate−polyacrylamide gel electrophoresis; SHE, standard hydrogen electrode; SCE, standard calomel electrode; SWV, square wave voltammetry; *T*, temperature; TAPS, *N*-[tris(hydroxymethyl)methyl]-3-aminopropanesulfonic acid; TMAO, trimethylammonium *N*-oxide.

10.1021/bi035869j CCC: $27.50
Published on Web 12/23/2003

paralogue of NarGHI and may be involved with the transition from aerobic to anaerobic conditions (*3*, *4*).

The structure of NarGHI has recently been solved by Bertero and co-workers (*5*). In overall architecture it is similar to the formate dehydrogenase complex, FdnGHI (*6*); this similarity is remarkable as it is proposed that NarGHI and FdnGHI function together in a redox loop to translocate protons across the cytoplasmic membrane (*5*, *6*). NarGHI contains a Mo-bisMGD cofactor, which is used to reduce cytoplasmic nitrate to nitrite. The Mo-bisMGD catalytic site of NarGHI has a number of unusual features (*5*). The protein−Mo ligand is provided by an unprecedented Asp residue, with both carboxylate oxygens within the coordination sphere of the Mo atom. As a result of this, and in contrast to the other structurally characterized Mo-bisMGD-containing enzymes (*6*−*9*), the Mo coordination sphere in NarGHI appears to lack an oxo group or hydroxyl oxygen in what is believed to be the oxidized state (*5*).

NarGHI utilizes a pair of *b* hemes bound in the transmembrane domain (NarI) and five iron−sulfur clusters contained (mostly) within the β subunit (NarH, 58 kDa) to convey electrons to the Mo-bisMGD active site in the membrane-extrinsic catalytic subunit (NarG, 139 kDa). The redox cofactors transfer electrons across a potential range from +420 mV (nitrate/nitrite at pH 7.0) to between −100 and +100 mV, depending on the quinone composition, menaquinol or ubiquinol (*10*). Redox titrations show that the Mo(V) state is stable over a wide potential region. For the "low-pH" form, the reduction potentials of the Mo(VI/V) and Mo(V/IV) couples were reported as > +450 and +200 mV, respectively, whereas for the "high-pH" form (at pH 8.1), the corresponding potentials were +250 and +90 mV (*11*). The reduction potentials for the four Fe-S clusters found in NarH and the two hemes in NarI have been measured by optical and/or EPR spectroscopy (*12*−*15*). Surprisingly, the reduction potentials of these Fe-S clusters span a range of more than +600 mV (+180 mV to −420 mV) (*13*, *16*). From the structure determination, it is now known that NarG also contains an Fe-S cluster, a [4Fe-4S] cluster with a novel His ligand, which has so far proven recalcitrant to spectroscopic examination (*5*).

Protein film voltammetry, electrochemistry of protein molecules confined to an electrode surface, is a highly effective approach for investigating redox enzymes and their mechanisms of catalysis (*17*). Provided that the supply of substrate to the electrode is not limiting and interfacial ET is fast, the catalytic current is a direct measure of the enzyme's activity. The redox states of different centers, and correspondingly the activities that may depend critically on these redox states, are easily controlled and varied *directly* by applying the electrode potential over a continuous range. Recently, Butt and co-workers used protein film voltammetry to examine the catalytic properties of a soluble form of nitrate reductase that is related to the *E. coli* enzyme, the NarGH subcomplex from *Paracoccus pantotrophus* (*18*, *19*). The catalytic voltammograms obtained for NarGH adsorbed on a PGE electrode were complex; most significantly, it was found that at low nitrate concentrations the activity decreases at higher driving force, i.e., as the electrode potential is made more negative. Different possibilities were proposed, one being that nitrate binds more tightly (K_M is lower) to the active site in the Mo(V) state compared to Mo(IV). This is an interesting proposal since little is established on how a substrate might select for different oxidation states of Mo cofactors, let alone the influence that potential (the electrochemical driving force) has on catalytic electron transport in general. In a recent study of *E. coli* DMSO reductase, which is also a multisubunit, multicenter membrane-bound enzyme, we observed a similar optimal activity suggesting a higher activity for Mo(V) (*20*).

In this paper, we present electrochemical investigations of the NarGHI holoenzyme from *E. coli*, for which the results also reveal a complex activity-potential dependence. To probe the origin of this behavior, we have used two inhibitors, azide and thiocyanate, to examine separately the different regions of the catalytic voltammograms. These are known to be competitive inhibitors of nitrate reduction and therefore provide direct probes for catalytic processes located at the Mo site. This paper presents a detailed examination of the catalytic and inhibited forms of NarGHI, which suggests a redox-sensitive model of substrate/inhibitor binding that provides insight into the mechanism of nitrate reduction.

MATERIALS AND METHODS

Preparation of Enzyme Samples. NarGHI was expressed in *E. coli* LCB2048, from which inner membranes containing amplified levels of NarGHI were prepared as described previously (*13*, *21*, *22*). Enzyme was purified from the membranes as follows: (i) Membranes were extracted at pH 7.0 with 1% Thesit (Sigma) in 50 mM MOPS, 5 mM EDTA, 10% glycerol, and 100 mM NaCl (pH 7.0). (ii) The extract was loaded onto a DEAE-Sepharose FF column (Amersham Pharmacia Biotech) previously equilibrated at pH 7.5 with 50 mM HEPES, 100 mM NaCl, 0.05% Thesit, and glycerol. (iii) The column was reequilibrated to pH 7.5 with the HEPES buffer, and protein was eluted with a NaCl gradient (100−400 mM). (iv) Enriched fractions were pooled, concentrated, and then diluted in a pH 6.5 buffer containing 50 mM MES, 100 mM NaCl, 0.05% Thesit, and 10% glycerol. This was then subjected to a further round of chromatography on a second DEAE-Sepharose column in the MES buffer. Peak fractions eluted from this second column were judged to be ≥95% pure on the basis of SDS−PAGE analyses. This procedure produced upward of 20 mg of NarGHI per liter of bacterial culture.

Electrochemical Measurements. All water used in electrochemical studies was purified with a Milli-Q system to a resistivity of 18 MΩ cm. Sodium nitrate, potassium thiocyanate, sodium chloride, sodium azide, and buffer components (HEPES, TAPS, MOPS, MES) were of analytical grade such as SigmaUltra or AnalaR from BDH. Cyclic voltammetry was performed with an Autolab potentiostat PGSTAT10 or 20 (Eco Chemie, Utrecht, The Netherlands) equipped with an analogue or digital generator and an ECD module. All data collection was performed using the GPES (Eco Chemie) software package, and data analysis was carried out using an in-house program, as described previously (*23*). The rotating disk electrode (RDE) was constructed using an embedded pyrolytic graphite cylinder oriented with one of the edge plane ends facing the solution (hence pyrolytic graphite "edge"; PGE) and was used in conjunction with an EG&G Model 636 electrode rotator. The all-glass cell was designed for a three-electrode configura-

tion: the counter electrode (positioned in the sample compartment) was a piece of platinum wire, while the reference was a standard calomel electrode (SCE) located in a long side arm (filled with 0.1 M NaCl) which was joined to the sample compartment via a Luggin capillary tip. The sample compartment was enclosed by a water jacket and thermostated using a Neslab circulator. All experiments were performed under anaerobic conditions in a glovebox (Vacuum Atmospheres) with $O_2 < 4$ ppm. Potentials were adjusted to correspond to the standard hydrogen electrode (SHE) scale using $E_{SHE} = E_{SCE} + 241$ mV (at 25 °C) (*24*).

For each set of experiments, a film of NarGHI on the PGE electrode was prepared by first polishing the PGE electrode with an aqueous slurry of alumina (1 micron, Buehler), sonicating it briefly in water, and then immersing it in an ~10 μM solution of NarGHI, containing 200 μg/mL polymyxin. The electrode was rotated slowly (50 rpm), and the potential was cycled between +240 mV and −450 mV vs SHE at a scan rate of 10 mV s^{-1} for 30 min. The electrode was then removed from the cell solution, rinsed, and returned to the cell after the buffer had been exchanged for a protein-free solution. Mixtures of buffer components, 20−40 mM, were selected to give stability over the desired pH range. The enzyme film was most stable between pH 6 and pH 8, and good stability was achieved over the temperature range 25−30 °C; these conditions allowed the catalytic responses for several concentrations of nitrate to be measured for the same film over several hours. Attempts to grow a film by either simply soaking an electrode in a dilute protein solution or painting on a concentrated solution (as has been demonstrated to be effective for the *Paracoccus* enzyme) did not yield such reproducible voltammetry (*18*). For studying the pH dependence, the PGE electrode coated with the enzyme film was transferred randomly between different solutions, while frequent checks were made with a standard (e.g., pH 7.0) which served as a reference to correct for film loss over the course of the experiment (*20*).

RESULTS

Dependence of Catalytic Rates on Nitrate Concentration and Electrode Potential. Figure 1 shows cyclic voltammograms recorded for a NarGHI film prepared on a PGE electrode as described above and exposed to increasing concentrations of nitrate at 30 °C and pH 7.0. The faradaic waveshapes observed for each nitrate concentration are independent of scan direction but display an intriguing complexity that is described further below. At sufficiently negative potential the current due to nitrate reduction reaches a limiting value with no significant residual slope. In the absence of substrate no signals due to reversible electron transfers to the enzyme's redox centers (nonturnover signals) could be observed by cyclic voltammetry, showing that the electroactive coverage must be very low. However, NarGHI adsorbed on the electrode is highly active: indeed, at low nitrate concentrations the current depends on the rate at which the electrode is rotated until this is sufficiently high to relieve substrate supply to the electrode as the determining step. For Figure 1, the electrode is rotating at 2100 rpm, well in the region for which there is no dependence on rotation rate. By ensuring that the electrode rotation rate was always sufficiently high, the nitrate concentration dependence of currents at different electrode potentials could be used to obtain values for the Michaelis constant, K_M. Similar results were obtained using a film prepared using a gold electrode modified with the alkanethiol 3-mercaptopropanol, although the electroactive coverage was poor and the film response was unstable over time. Experiments were also carried out using the complete inner membrane fraction, and the voltammetry obtained at a PGE electrode showed the same features as did the purified enzyme. Samples of a NarGH-His_6 construct, devoid of the NarI subunit, gave similar results, though the film was less stable in the absence of NarI. Thus, the catalytic activity and the complex shape are not dependent on the presence of NarI. All further experiments were carried out by adsorbing purified NarGHI on PGE electrodes.

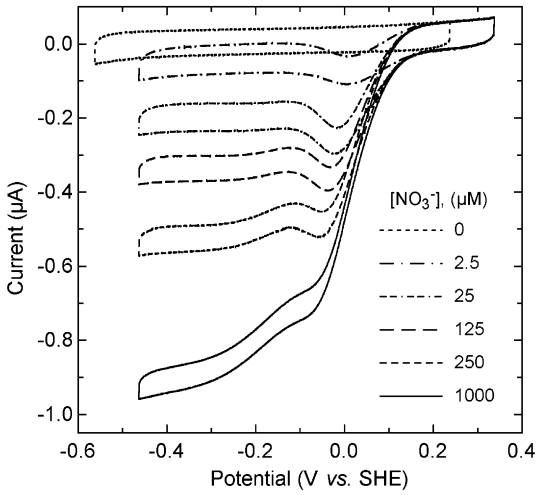

FIGURE 1: Catalytic response of a film of NarGHI on a PGE electrode in the presence of different concentrations of nitrate at 30 °C and pH 7.0. Cycles (10 mV/s) were initiated at the positive potential limit, and the electrode was rotated at 2100 rpm. A typical background cycle with a polished PGE electrode is included for comparison. Nitrate was added as small (microliter) volumes of a concentrated $NaNO_3$ stock solution to a cell solution of 2 mL volume.

Figure 2A shows the results for experiments at pH 7.0, 25 °C, spanning a nitrate concentration range 0.1−3 mM. To aid comparison and simplify the figure, only the scan in the positive direction is shown, and the background capacitance contribution has been subtracted. At low nitrate concentrations the voltammetry is dominated by a prominent reduction current maximum (this appears as a negative peak) at a potential of approximately −25 mV. This activity drops away quite sharply as the potential is lowered. As the nitrate concentration is raised the reduction current peak maximum shifts to lower potentials, but the main observation is that there is a marked increase in catalytic activity at more negative potentials. The voltammetry is eventually dominated by a large sigmoidal component at low potential that moves to more negative values as nitrate is added, although the shift is quite small (less than 50 mV as gauged from the half-wave potentials for experiments with 0.2 and 3.2 mM). Eventually the limiting current is reached at potentials below −300 mV, and in this limit the high potential activity appears as a smaller sigmoidal wave superimposed on the main wave. The results resemble those reported earlier for nitrate reductase from *P. pantotrophus*, but the high- and low-potential activities are better separated. The fact that there is little residual slope at the lower potential limit suggests

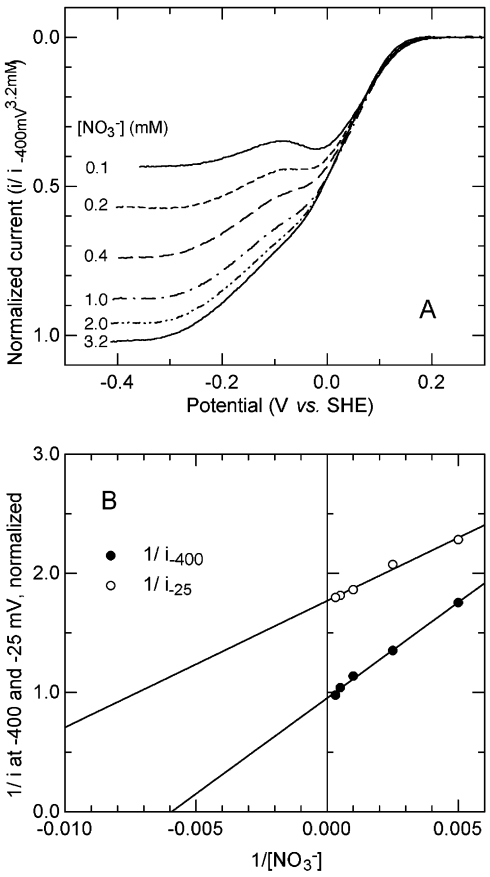

FIGURE 2: Nitrate dependence of the catalytic activity of NarGHI at pH 7.0 and 25 °C (other conditions as for Figure 1). (A) Voltammograms after background subtraction, normalized against the maximum current observed for a NarGHI film in the presence of 3.2 mM nitrate. For clarity, only the scan in the positive direction is shown. (B) Lineweaver−Burk plots for the catalytic activities observed at −25 mV (empty circles) or −400 mV (filled circles).

strongly that interfacial electron transfer is sufficiently fast so as not to influence the shape of the catalytic voltammogram (*25*).

The nitrate dependences of the two potential regions can be analyzed using a Michaelis−Menten model. The high-potential activity was measured from the current reading at a constant high potential (−25 mV) while the low-potential activity was determined from the current at low potential (−400 mV). Data were collected by monitoring the increase in reductive current with successive additions of nitrate, taking care that there was negligible overall loss of activity (current) throughout the course of the titration. The results were used to construct a Lineweaver−Burk plot, which is shown in Figure 2B and analyzed in terms of the Michaelis−Menten equation. Average values of K_M for several substrate titrations were 41 and 161 μM for the high- and low-potential activities, respectively. By comparing the two plots, the turnover number (k_{cat}) for the low-potential activity is approximately twice that observed at high potential.

Attempts to generate nonturnover signals in cyclic voltammetry experiments were unsuccessful: varying the pH, temperature, ionic strength, buffer concentration, and the inclusion or absence of other coadsorbates known to stabilize electroactive protein films (such as Mg^{2+}, neomycin, or tobramycin) did not lead to nonturnover signals. The most plausible explanation for this is that the electroactive coverage (the surface density of enzyme molecules actually able to exchange electrons easily with the electrode) is too low. Alternatively, the population of adsorbed enzyme molecules might be significantly heterogeneous, thus broadening the signals beyond detection; however, the excellent and well-defined catalytic voltammetry that is observed suggests that this is not the case. Considering the large number of redox centers in the enzyme, this suggests that the coverage is below 1 pmol cm^{-2} (*17*). From this value and a typical maximum current of 1 μA, the turnover number at high and low potentials is estimated to be at least 90 and 170 s^{-1}, respectively.[2] Weak nonturnover signals were observed using square-wave voltammetry, which provides amplification because the potential is modulated (*27*−*29*). The square-wave voltammograms consisted of a broad envelope of two overlapping weak signals between +100 and −300 mV, which will be brought into discussion later.

pH Dependence of Catalytic Activity. The pH dependence of the NarGHI catalytic waveforms was investigated at a high (2 mM) concentration of nitrate. As described above, catalytic reduction waves were observed over the pH range 5.0−9.0, and the electrochemistry was sufficiently stable that a single film could be used to obtain all of the measurements. Data for each pH were corrected for film loss and normalized with respect to the maximum limiting current observed at pH 5.0. Results from several experiments were reproducible. The scans from complete data sets are shown in Figure 3A. Only the scans in the negative direction are shown, and the background capacitance has been subtracted to aid comparison. There are large variations in current as a function of pH, with maximum activity occurring at pH 5.0. Due to poor film stability, data for lower pH values were not used. The two regions of the catalytic wave identified earlier were now analyzed separately by measuring the potential values corresponding to the half-wave potential of each component sigmoid (this was facilitated by determining the derivative di/dE). The high-potential activity is centered at a potential $E_{cat}(1)$ while the low-potential activity is associated with a potential $E_{cat}(2)$. From the broad widths of the peak shapes in the derivative of the voltammogram, the electron cooperativity over both regions of activity is low, suggesting a discrete one-electron rate-limiting step for the two-electron transfer reaction. As the pH is raised, $E_{cat}(1)$ shifts to more negative potential (Figure 3B) whereas $E_{cat}(2)$ does not change with pH. The data obtained for the variation of $E_{cat}(1)$ with pH gave a good fit to eq 2 in which E_{acid} is the

$$E_{cat}(1) = E_{acid} - \frac{2.3RT}{nF}\log(1 + K_{ox}/a_{H^+}) \qquad (2)$$

limiting (upper) value at low pH, K_{ox} is the acid dissociation constant for the oxidized form of the redox couple, a_{H^+} is the proton activity (pH = −log a_{H^+}), and the other terms are defined in footnote 1. We obtained E_{acid} = 35 mV and pK_{ox} = 7.8. In other words, the high-potential catalytic process is dependent on a species that undergoes a reversible acid−base transition in the oxidized form with pK_{ox} = 7.8, below which no net reversible proton transfer is involved

[2] The turnover number is estimated from the limiting current, i_{lim}, at saturating substrate concentration using the relationship $k_{cat} = i_{lim}/nA\Gamma F$, where Γ represents the electroactive surface coverage for the enzyme on an electrode of surface area A (*26*).

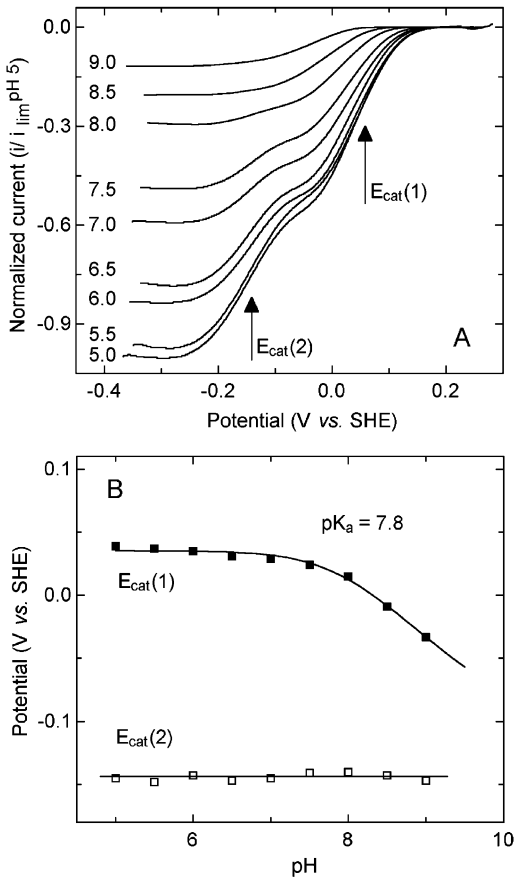

FIGURE 3: (A) Background-corrected voltammograms for nitrate reduction by NarGHI measured at 2 mM nitrate over a range of pH (other conditions as for Figure 1). (B) Plot showing the variation with pH of half-wave potentials for both the high-potential activity, $E_{cat}(1)$, and for the low-potential activity, $E_{cat}(2)$.

and the catalytic activity (the current) is large. By contrast, the zero pH dependence of $E_{cat}(2)$ shows that this pathway involves catalytic species that do not change their protonation states over the pH range 5−9. Significantly, both of these components appear at potentials far more negative than the two-electron NO_3^-/NO_2^- couple (+420 mV), which is a two-proton reaction; consequently, the catalytic action being observed by voltammetry is determined by the characteristics of the enzyme rather than the substrate.

Experiments with Inhibitors. To identify the origin of the variations in catalytic activity as a function of potential, we carried out experiments in the presence of inhibitors. First, we examined the effect of adding nitrite, the reaction product. This gave no change in the voltammetry, so we could conclude that its binding is very weak and it is not responsible for the unusual waveform observed. Experiments with and without 100 mM chloride also showed little difference, consistent with the reported K_d for chloride of 0.5 M (*30*). However, the results were strikingly different when we tested the effect of two known competitive inhibitors of nitrate reduction, azide (*31*) and thiocyanate (*32*). Figure 4 shows the effect of 1 μM azide on the voltammograms measured for different nitrate concentrations. Comparison of the results obtained for 100 μM nitrate with and without azide shows that both high- and low-potential activities are almost abolished by azide; however, when the nitrate concentration is raised to 1 mM, only the low-potential activity makes any significant contribution to the voltammetry. This observation was investigated further (Figure 5A) by recording the catalytic voltammograms for varying concentrations of nitrate in the presence of 3 μM azide. These showed that even with nitrate as high as 6 mM, there is little recovery of the activity at higher potential.

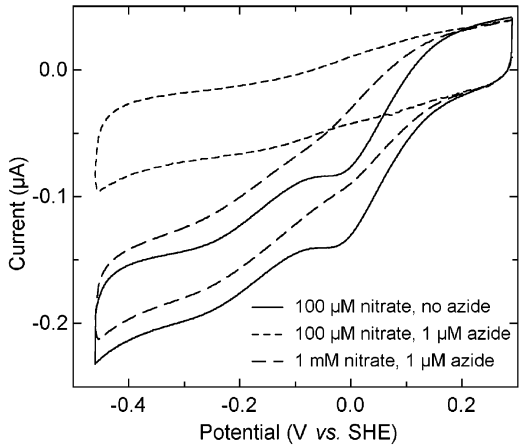

FIGURE 4: Effect of azide on the catalytic voltammetry of NarGHI measured at pH 7.0 and 25 °C (other conditions as in Figure 1). Voltammograms were recorded with the same film of NarGHI on a PGE electrode with nitrate and azide levels adjusted by microliter addition of appropriate stock solutions to the 2 mL cell volume.

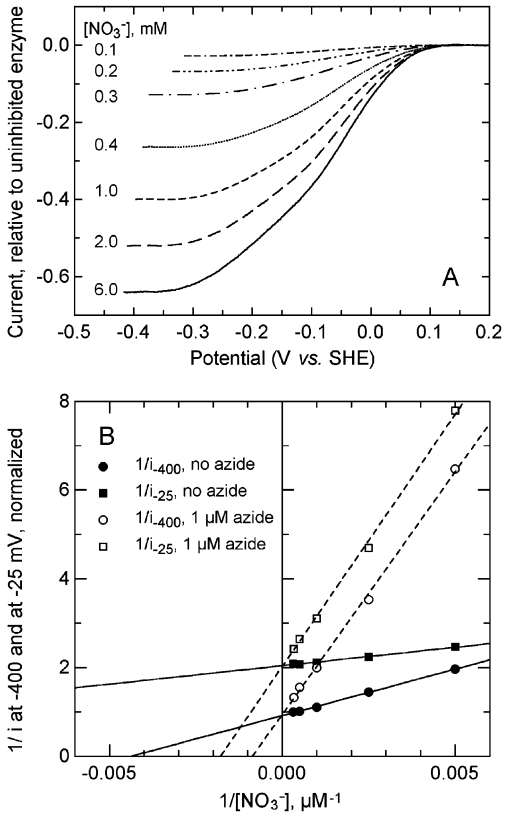

FIGURE 5: (A) Catalytic voltammograms at pH 7.0 and 25 °C, background-corrected and normalized with respect to the activity of the uninhibited enzyme with 3.2 mM nitrate, showing the effect of nitrate concentration on the waveshapes obtained in the presence of 3 μM azide. (B) Lineweaver−Burk plots based on the normalized currents measured for high-potential (−25 mV) and low-potential (−400 mV) activities, both with and without azide. The shared *y*-intercepts show that azide is fully competitive with nitrate at both potentials; this was seen for both 1 and 3 μM azide (the latter is omitted for clarity). The shifts in the *x*-intercepts show that the apparent K_M increases with increasing azide concentration, with the effect greater at −25 mV.

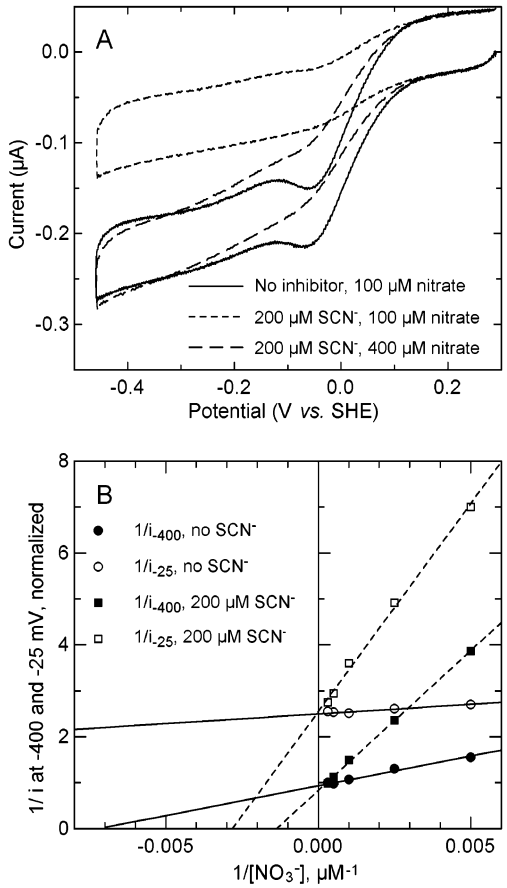

FIGURE 6: (A) Effect of thiocyanate on the catalytic voltammetry of NarGHI measured at pH 7.0 and 25 °C (other conditions as in Figure 1). Adding 200 μM thiocyanate to a solution containing 400 μM nitrate results in a decrease in activity, as well as a simplification of the shape of the voltammogram. Increasing the substrate concentration to 1.6 mM restores activity but not the full level of enhanced activity at higher potentials exhibited by the uninhibited enzyme. (B) Lineweaver−Burk plots based on the currents measured for high-potential (−25 mV) and low-potential (−400 mV) activities, both with and without thiocyanate (results for 600 μM thiocyanate omitted for clarity).

A quantitative analysis of the inhibition characteristics was carried out by measuring the currents at high (−25 mV) and low (−400 mV) potentials as functions of both nitrate and azide concentrations. The results are shown in Figure 5B in the form of Lineweaver−Burk plots. The data give excellent fits, with the coincidence of *y*-axis intercepts for data obtained at either potential showing that azide acts competitively in both the high- and low-potential activities. The presence of the inhibitor causes a large increase in the apparent Michaelis constant, K_M, for nitrate as determined from the *x*-intercepts in the plot, with the greater effect occurring for the data at −25 mV, indicating much tighter binding of azide at higher potential. The increased value for K_M, K_M^{app}, was used to find the competitive inhibition constant, K_d, for azide at each potential for both 1 and 3 μM azide according to a standard treatment (*33*): $K_M^{app} = K_M(1 + [I]/K_d)$. The average K_d values for high and low potentials are 0.08 and 0.22 μM, respectively.

Similar experiments were carried out with thiocyanate. Figure 6A shows the effect of 0.2 mM thiocyanate on the voltammetry of 0.4 and 1.6 mM nitrate. Thiocyanate is a much weaker inhibitor than azide, requiring much higher concentrations to have an appreciable effect. The resulting Lineweaver−Burk plots are shown in Figure 6B; an analysis as before gives average K_d values of 11 and 33 μM for high and low potentials, respectively. The average results obtained from several measurements of the different substrate and inhibitor binding constants are summarized in Table 1. Also tabulated are different ratios that are of interest in this study, i.e., ratios of Michaelis/dissociation constants for nitrate/inhibitors and ratios of low-potential/high-potential binding constants.

DISCUSSION

Two Different Activities for Nitrate Reductase. The NarGHI holoenzyme adsorbed on a PGE electrode displays catalytic voltammetry that is stable for long periods at 30 °C, even when no additional enzyme is present in the cell solution. The electroactive coverage is too low to enable nonturnover signals to be observed by cyclic voltammetry, but when substrate is added the catalytic activity is sufficiently high that the signal from even a small population of enzyme is greatly amplified. The exact form in which the enzyme is adsorbed is not known, but the observations (a) that a similar but attenuated response is obtained at a modified gold electrode and (b) that a soluble construct lacking the NarI subunit also gives a similar catalytic wave together suggest strongly that the results are reporting on the inherent properties of the NarGH subcomplex and not those of the electrode interface or the membrane domain. It is possible that adsorption on PGE causes the complex to separate into its individual subunits, but it is clear that whatever processes occur, the resulting enzyme is very active and the catalytic components are unlikely to be altered. Similar results were obtained over the course of many experiments, including using NarGHI samples from different preparations. Therefore it is most unlikely that the high- and low-potential activities are a result of different states of the enzyme.

The observation of two different reactivities for nitrate reductase, one optimized within a narrow high-potential region and one reaching a sigmoidal maximum at low potential, is the central feature of this study. At pH 7.0, the rate of turnover at the higher potential is approximately one-half that at low potential, whereas the value of K_M is approximately four times less. This observation is similar to that reported earlier for the *P. pantotrophus* enzyme by Butt and co-workers, who considered different ways in which the complex catalytic waveform might arise (*18*, *19*). Apart from processes occurring at the Mo site, other possibilities were that the rate of catalysis is sensitive to the redox state of an Fe-S cluster or that two distinct active conformations of the NarGHI protein exist on the electrode, one of which is less active, yet more populated at lower reduction potential. However, while these other possibilities could easily explain a potential dependence for the rate of turnover, they are more difficult to reconcile with the apparent potential dependence of the nitrate binding affinity.

Analysis of the Potential-Dependent Activities. The definitive information we are now able to provide is the effect on the waveform of adding a competitive inhibitor such as azide. The results not only show that azide is a competitive inhibitor of nitrate reductase bound to an electrode just as it is in solution but also reveal that the inhibitory effect is especially

Table 1: Compilation of Michaelis and Inhibition Constants for Nitrate Reductase[a]

	$K_M(NO_3^-)/\mu M$	$K_d(N_3^-)/\mu M$	ratio (K_M/K_d)	$K_d(SCN^-)/\mu M$	ratio (K_M/K_d)
high potential	41 ± 26	0.08 ± 0.05	510	11 ± 7	3.7
low potential	161 ± 39	0.22 ± 0.02	730	33 ± 11	4.9
affinity ratio	3.9 ± 1.9	2.8 ± 0.6		3.0 ± 0.7	

[a] Average values are provided with standard deviations at both high (−25 mV) and low (−400 mV) potential for ten measurements of K_M and six measurements of K_d representing two different concentrations for each inhibitor.

pronounced for the high-potential activity. At high potential, azide binds more than 2 orders of magnitude more tightly than nitrate; furthermore, it is selective for the high-potential activity by a factor of 3 over the low-potential activity. This fact in particular provides compelling evidence that the potential dependence reflects the differing catalytic properties of two oxidation states of the active site, at which competitive inhibition must occur. If instead the catalytic voltammetry were controlled by the oxidation states of one or more Fe-S clusters or indeed any more remote aspect of the enzyme, it would be most unlikely that azide could exert such a high level of discrimination in its inhibition of high-potential activity. Azide binds much more tightly than thiocyanate, which is also more selective for the high-potential activity but with a binding affinity only four times greater than that of nitrate. In terms of "hard−soft" characteristics, it is well established that azide is a harder ligand than thiocyanate and is therefore expected to show a relative preference for metal ions in higher oxidation states.

The pH dependence of the catalytic waveforms shows that there is a general increase in activity (current) with decreasing pH; however, only the high-potential activity exhibits a pH-potential dependence, and this is associated with an ionization in the oxidized form with $pK_{ox} = 7.8$. Magalon and co-workers examined the Mo(V) states of NarGHI as a function of pH using EPR spectroscopy, finding two forms of the Mo(V) signal that were related by a pK_a of 7.4 (*11*). Notably, the reduction potentials for both Mo(VI)/(V) and Mo(V)/(IV) redox couples observed in their study (+190 and + 95 mV, respectively) were considerably higher than the regions of catalytic activity we now observe. However, in our studies different quantities are being measured, and importantly, the two kinds of measurements are made under very different conditions: equilibrium measurements on concentrated membrane preparations frozen in an EPR tube, compared to ambient temperature rate measurements with enzyme molecules adsorbed on an electrode, for which the potential being applied is that required to maintain a catalytic steady state of *electron flow to substrate* rather than a reversible stoichiometric equilibrium. Our own arguments are based not on any direct and unambiguous observation of Mo(V) but on catalytic activity that implicates the active site on account of the sensitivity to competitive inhibitors, particularly azide. One other possibility is that our measurements are necessarily made in the presence of nitrate, which is not present in the EPR samples. However, the shifts in potential with increasing nitrate concentration are small, so if nitrate were the factor responsible for lowering the Mo reduction potentials, then an additional "nonsubstrate" nitrate ion (i.e., one not being catalytically reduced) would have to be bound very tightly to oxidized forms of the enzyme. Experiments carried out in the absence of nitrate using square wave voltammetry showed a weak envelope of signals between +100 and −300 mV, the positions of which changed upon addition of azide; however, it was not possible to make a definite assignment, as the large width of the signal (> +400 mV) clearly demonstrated that it arose from multiple redox species, very likely including the Fe-S clusters and/or heme groups of NarGHI.

Redox Transitions at the Active Site. It is also possible that the potential dependence of activity that we observe arises not from the Mo(V) itself but from redox chemistry associated with the pterin ligands. The bicyclic form observed for one of the molybdopterin cofactors in the NarGHI crystal structure (*5*) could represent the tetrahydropterin form that is two hydrogen atoms more reduced than the tricyclic form observed for the other molybdopterin in NarGHI as well as for those in all other crystallographically characterized molybdopterin-containing enzymes (*34*). The intriguing possibility is that reversible reduction of the pterin occurs (not necessarily as a direct part of the catalytic mechanism) and that this decreases the binding affinity at molybdenum for substrate and inhibitors, giving a sharp two-electron switch in the voltammetry. However, determination by voltammetry of the electron cooperativity for an on/off switch is difficult (*20*, *35*), as it is possible that the shape of the voltammogram results from the balance of the many other factors involved in modeling the waveform (*18*). Furthermore, ring opening of the pterin can also occur by a rearrangement/scission mechanism without any change in redox level of the pterin (*34*). Apart from one paper reporting formation of a pterin radical (*36*), we are not aware of observations so far to suggest that the pterin ligands associated with Mo undergo redox transitions during catalysis; but in the absence of crystallographic characterization of both the reduced and oxidized states of the enzyme, it remains possible that such a transition could occur in this system.

Assuming that redox transitions of the Mo atom are the most likely origin of the potential dependence, our simplified attempt to explain the catalytic data is shown in Scheme 1. As required for nitrate reduction, both the high- and low-potential activities must involve two electrons and two protons. Further assumptions made are that the Mo cycles between oxidation states VI and IV and that even if nitrate binds to Mo(VI) [we note that there is only a relatively small shift in $E_{cat}(1)$ with increasing nitrate concentration], the potential region in which this occurs does not provide sufficient reducing power to give a detectable rate of catalysis. Of the net number of protons required in the catalytic cycle and taken up from solvent, only one is involved in any potential-determining process, that of $E_{cat}(1)$, which is associated with a pK_{ox} value of 7.8. Thus, below pH 7, the rate (current) but not the potential is dependent on pH. This allows us to separate two protonation steps, one occurring as a fast preequilibrium and one required for the formation and release of product. Since there is no pH dependence for $E_{cat}(2)$, it follows that the same number

Scheme 1: Proposed Pathways (in Bold) for Nitrate Reduction Based on Voltammetric Evidence Reported in This Investigation[a]

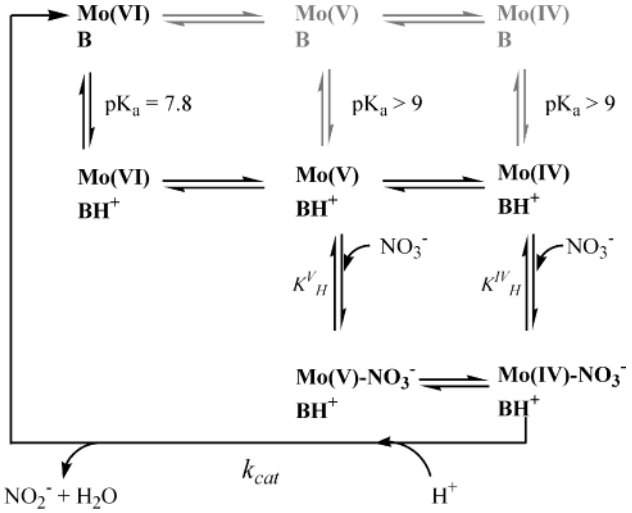

[a] B denotes a general base that undergoes protonation at the oxidized active site with pK_a 7.8.

of protons are bound for both oxidation states involved. We will assign these as Mo(V) and Mo(IV). It then follows that the pK_{ox} for $E_{cat}(1)$ must be assigned to the active site in the oxidation state Mo(VI). It should be stressed at this stage that we cannot assign this proton-transfer equilibrium to any particular site: it does not have to be at the Mo but only at a site that is crucial for catalysis and close enough for its pK to be controlled by the Mo oxidation state. Thus it need not be correlated with any acid−base equilibrium previously detected, e.g., by EPR.

The following predictions are then made. One exchangeable proton, crucial for both high- and low-potential activities, is bound under all conditions, except to Mo(VI) at pH >7.8. At low nitrate concentration, Mo(V) plays a major role in the catalytic cycle because it has a higher affinity for nitrate than Mo(IV). Once nitrate has bound to Mo(V), the cycle continues with the addition of a further electron and proton, and product is released. At higher nitrate levels, an alternative pathway that involves nitrate binding to Mo(IV) and a higher rate of turnover becomes dominant. At pH values above 8, the high-potential pathway with nitrate entering the cycle at Mo(V) loses significance as $E_{cat}(1)$ becomes close to $E_{cat}(2)$. The results contrast with those obtained for a different enzyme, DMSO reductase, for which the substrate concentration makes little difference to the observations of the high- and low-potential signals (*20*).

Biological Implications. The results show that a considerable amount of energy (approximately 2 × 0.4 F, i.e., 80 kJ/mol of nitrate) is expended in the reductive half-cycle, making this an inefficient but irreversible process. More subtle, however, is the way in which the catalytic activity differs across two potential domains. In *E. coli*, the natural electron donors range from menaquinol to ubiquinol depending on factors such as anaerobicity and availability of terminal oxidants. The results suggest that low levels of nitrate can be reduced using ubiquinol, the electron donor prevailing under aerobic conditions, and this might also be useful under some intermediate growth conditions. They also suggest that this high-potential activity is the one most susceptible to azide inhibition. This may have interesting implications for the practical applications of inhibitors, as in bacteriostatic preservatives.

ACKNOWLEDGMENT

We are grateful to Drs. Francis Blasco and Nicolas Ginet, Laboratoire de Chimie Bactérienne, IBSM, CNRS, Marseille, for help in preparing enzyme samples.

REFERENCES

1. Richardson, D. J. (2000) Bacterial respiration: A flexible process for a changing environment, *Microbiology 146*, 551−571.
2. Hille, R. (1996) The mononuclear molybdenum enzymes, *Chem. Rev. 96*, 2757−2816.
3. Blasco, F., Iobbi, C., Ratouchniak, J., Bonnefoy, V., and Chippaux, M. (1990) Nitrate reductases of *Escherichia coli*—sequence of the 2nd nitrate reductase and comparison with that encoded by the narGHJI operon, *Mol. Gen. Genet. 222*, 104−111.
4. Iobbi, C., Santini, C. L., Bonnefoy, V., and Giordano, G. (1987) Biochemical and immunological evidence for a 2nd nitrate reductase in *Escherichia coli* K12, *Eur. J. Biochem. 168*, 451−459.
5. Bertero, M. G., Rothery, R. A., Palak, M., Hou, C., Lim, D., Blasco, F., Weiner, J. H., and Strynadka, N. C. J. (2003) Insights into the respiratory electron-transfer pathway, *Nat. Struct. Biol. 10*, 681−687.
6. Jormakka, M., Tornroth, S., Byrne, B., and Iwata, S. (2002) Molecular basis of proton motive force generation: Structure of formate dehydrogenase-N, *Science 295*, 1863−1868.
7. Schindelin, H., Kisker, C., Hilton, J., Rajagopalan, K. V., and Rees, D. C. (1996) Crystal structure of DMSO reductase: Redox-linked changes in molybdopterin coordination, *Science 272*, 1599−1600.
8. Dias, J. M., Than, M. E., Humm, A., Huber, R., Bourenkov, G. P., Bartunik, H. D., Bursakov, S., Calvete, J., Caldeira, J., Carneiro, C., Moura, J. J. G., Moura, I., and Romao, M. J. (1999) Crystal structure of the first dissimilatory nitrate reductase at 1.9 Å solved by MAD methods, *Struct. Folding Des. 7*, 65−79.
9. Ellis, P. J., Conrads, T., Hille, R., and Kuhn, P. (2001) Crystal structure of the 100 kDa arsenite oxidase from *Alcaligenes faecalis* in two crystal forms at 1.64 Å and 2.03 Å, *Structure 9*, 125−132.
10. Wissenbach, U., Kroger, A., and Unden, G. (1990) The specific functions of menaquinone and demethylmenaquinone in anaerobic respiration with fumarate, dimethyl sulfoxide, trimethylamine *N*-oxide and nitrate by *Escherichia coli*, *Arch. Microbiol. 154*, 60−66.
11. Magalon, A., Asso, M., Guigliarelli, B., Rothery, R. A., Bertrand, P., Giordano, G., and Blasco, F. (1998) Molybdenum cofactor properties and Fe-S cluster coordination in *Escherichia coli* nitrate reductase A: Investigation by site-directed mutagenesis of the conserved His-50 residue in the NarG subunit, *Biochemistry 37*, 7363−7370.
12. Magalon, A., Lemesle-Meunier, D., Rothery, R. A., Frixon, C., Weiner, J. H., and Blasco, F. (1997) Heme axial ligation by the highly conserved His residues in helix II of cytochrome b (NarI) of *Escherichia coli* nitrate reductase A (NarGHI), *J. Biol. Chem. 272*, 25652−25658.
13. Rothery, R. A., Magalon, A., Giordano, G., Guigliarelli, B., Blasco, F., and Weiner, J. H. (1998) The molybdenum cofactor of *Escherichia coli* nitrate reductase A (NarGHI)—effect of a MobAB mutation and interactions with Fe−S clusters, *J. Biol. Chem. 273*, 7462−7469.
14. Guigliarelli, B., Magalon, A., Asso, M., Bertrand, P., Frixon, C., Giordano, G., and Blasco, F. (1996) Complete coordination of the four Fe-S centers of the beta subunit from *Escherichia coli* nitrate reductase. Physiological, biochemical, and EPR characterization of site-directed mutants lacking the highest or lowest potential 4Fe-4S clusters, *Biochemistry 35*, 4828−4836.
15. Hackett, N. R., and Bragg, P. D. (1982) The association of two distinct b cytochromes with the respiratory nitrate reductase of *Escherichia coli*, *FEMS Microbiol. Lett. 13*, 213−217.
16. Guigliarelli, B., Asso, M., More, C., Augier, V., Blasco, F., Pommier, J., Giordano, G., and Bertrand, P. (1992) EPR and redox characterization of iron−sulfur centers in nitrate reductases-A and reductases-Z from *Escherichia coli*—evidence for a high-potential

and a low-potential class and their relevance in the electron-transfer mechanism, *Eur. J. Biochem. 207*, 61−68.
17. Léger, C., Elliott, S. J., Hoke, K. R., Jeuken, L. J. C., Jones, A. K., and Armstrong, F. A. (2003) Enzyme electrokinetics: Using protein film voltammetry to investigate redox enzymes and their mechanisms, *Biochemistry 42*, 8653−8662.
18. Anderson, L. J., Richardson, D. J., and Butt, J. N. (2001) Catalytic protein film voltammetry from a respiratory nitrate reductase provides evidence for complex electrochemical modulation of enzyme activity, *Biochemistry 40*, 11294−11307.
19. Anderson, L. J., Richardson, D. J., and Butt, J. N. (2000) Using direct electrochemistry to probe rate-limiting events during nitrate reductase turnover, *Faraday Discuss.*, 155−169.
20. Heffron, K., Leger, C., Rothery, R. A., Weiner, J. H., and Armstrong, F. A. (2001) Determination of an optimal potential window for catalysis by *E. coli* dimethyl sulfoxide reductase and hypothesis on the role of Mo(V) in the reaction pathway, *Biochemistry 40*, 3117−3126.
21. Rothery, R. A., Blasco, F., Magalon, A., Asso, M., and Weiner, J. H. (1999) The hemes of *Escherichia coli* nitrate reductase A (NarGHI): Potentiometric effects of inhibitor binding to NarI, *Biochemistry 38*, 12747−12757.
22. Augier, V., Guigliarelli, B., Asso, M., Bertrand, P., Frixon, C., Giordano, G., Chippaux, M., and Blasco, F. (1993) Site-directed mutagenesis of conserved cysteine residues within the beta-subunit of *Escherichia coli* nitrate reductase—physiological, biochemical, and EPR characterization of the mutated enzymes, *Biochemistry 32*, 2013−2023.
23. Léger, C., Heffron, K., Pershad, H. R., Maklashina, E., Luna-Chavez, C., Cecchini, G., Ackrell, B. A. C., and Armstrong, F. A. (2001) Enzyme electrokinetics: Energetics of succinate oxidation by fumarate reductase and succinate dehydrogenase, *Biochemistry 40*, 11234−11245.
24. Bard, A. J., and Faulkner, L. R. (2001) *Electrochemical methods: Fundamentals and applications*, 2nd ed., John Wiley & Sons, New York.
25. Léger, C., Jones, A. K., Albracht, S. P. J., and Armstrong, F. A. (2002) Effect of a dispersion of interfacial electron-transfer rates on steady state catalytic electron transport in NiFe-hydrogenase and other enzymes, *J. Phys. Chem. B 106*, 13058−13063.
26. Heering, H. A., Hirst, J., and Armstrong, F. A. (1998) Interpreting the catalytic voltammetry of electroactive enzymes adsorbed on electrodes, *J. Phys. Chem. B 102*, 6889−6902.
27. Odea, J. J., and Osteryoung, J. G. (1993) Characterization of quasi-reversible surface processes by square-wave voltammetry, *Anal. Chem. 65*, 3090−3097.
28. Jeuken, L. J. C., McEvoy, J. P., and Armstrong, F. A. (2002) Insights into gated electron-transfer kinetics at the electrode-protein interface: A square wave voltammetry study of the blue copper protein azurin, *J. Phys. Chem. B 106*, 2304−2313.
29. Jeuken, L. J. C., Jones, A. K., Chapman, S. K., Cecchini, G., and Armstrong, F. A. (2002) Electron-transfer mechanisms through biological redox chains in multicenter enzymes, *J. Am. Chem. Soc. 124*, 5702−5713.
30. George, G. N., Bray, R. C., Morpeth, F. F., and Boxer, D. H. (1985) Complexes with halide and other anions of the molybdenum center of nitrate reductase from *Escherichia coli*, *Biochem. J. 227*, 925−931.
31. Butler, C. S., Charnock, J. M., Bennett, B., Sears, H. J., Reilly, A. J., Ferguson, S. J., Garner, C. D., Lowe, D. J., Thomson, A. J., Berks, B. C., and Richardson, D. J. (1999) Models for molybdenum coordination during the catalytic cycle of periplasmic nitrate reductase from *Paracoccus denitrificans* derived from EPR and EXAFS spectroscopy, *Biochemistry 38*, 9000−9012.
32. Butler, C. S., Charnock, J. M., Garner, C. D., Thomson, A. J., Ferguson, S. J., Berks, B. C., and Richardson, D. J. (2000) Thiocyanate binding to the molybdenum centre of the periplasmic nitrate reductase from *Paracoccus pantotrophus*, *Biochem. J. 352*, 859−864.
33. Cornish-Bowden, A. (1995) *Fundamentals of enzyme kinetics*, Portland Press, London.
34. Enemark, J. H., and Garner, C. D. (1997) The coordination chemistry and function of the molybdenum centres of the oxomolybdoenzymes, *J. Biol. Inorg. Chem. 2*, 817−822.
35. Elliott, S. J., Leger, C., Pershad, H. R., Hirst, J., Heffron, K., Ginet, N., Blasco, F., Rothery, R. A., Weiner, J. H., and Armstrong, F. A. (2002) Detection and interpretation of redox potential optima in the catalytic activity of enzymes, *Biochim. Biophys. Acta 1555*, 54−59.
36. Hurshman, A. R., Krebs, C., Edmondson, D. E., Huynh, B. H., and Marletta, M. A. (1999) Formation of a pterin radical in the reaction of the heme domain of inducible nitric oxide synthase with oxygen, *Biochemistry 38*, 15689−15696.

BI035869J